Applied Catalysis B: Environmental 162 (2015) 227–235

Contents lists available at ScienceDirect

Applied Catalysis B: Environmental

journal homepage: www.elsevier.com/locate/apcatb

Deep oxidation of chlorinated VOCs over CeO_2-based transition metal mixed oxide catalysts

Peng Yang, Shanshan Yang, Zhinan Shi, Zhonghua Meng, Renxian Zhou*

Institute of Catalysis, Zhejiang University, Hangzhou 310028, PR China

ARTICLE INFO

Article history:
Received 14 April 2014
Received in revised form 6 June 2014
Accepted 26 June 2014
Available online 5 July 2014

Keywords:
Chlorinated VOCs
Catalytic oxidation
CeO_2
Transition metal
Mixed oxides

ABSTRACT

Cerium-transition metal mixed oxides (4Ce1M, M = V, Cr, Mn, Fe, Co, Ni and Cu) were prepared by coprecipitation method and investigated for deep oxidation of four chlorinated VOCs with quite different molecule structures. 4Ce1M catalysts show mesoporous structures with larger specific surface area and pore volume, and some metal ions can go into the lattice of fluorite, which contributes to improving the stability of the active components. The redox properties of 4Ce1M catalysts are significantly promoted due to the strong interaction between CeO_2 and MO_x, which facilitates the destruction of the reactants and byproducts at lower temperature in the process of CVOCs oxidation. Especially, 4Ce1Cr catalyst exhibits the best catalytic activity and selectivity, mainly due to the formation of Cr^{6+} species with strong oxidizing ability. 4Ce1Cr also represents good durability for DCE destruction during the 100 h continuous test, and the chemical adsorbed Cl species on the surface can be removed above 325 °C. Moreover, the presence of water or non-chlorinated VOCs can slightly decrease the conversion of chlorinated VOCs at lower temperature due to the competitive adsorption for active sites, while promote at higher temperature (above 300 °C) because of the contribution to removing Cl species away from the surface.

1. Introduction

Chlorinated volatile organic compounds (CVOCs or chlorinated VOCs), consist of a wide range of solvents and intermediates commonly used in chemical industry, and are released into the atmosphere from lots of industrial operations [1–3]. These compounds are well known for their suspected toxicity and carcinogenic properties to human beings, and tend to accumulate in the environment [2]. Catalytic oxidation has been adopted as one of the most widely strategies to eliminate CVOCs emissions, mainly due to its much lower energy consumption compared to thermal combustion [4]. And catalytic oxidation can also control the emissions of NO_x and polychlorinated aromatics at the same time, since the reaction temperatures are lower than those at which NO_x can be formed [5].

The main catalysts for catalytic oxidation of CVOCs are supported noble metals and metal oxides. Generally, literatures reported before show that supported noble metal catalysts represent higher activity and selectivity to CO_x than metal oxides catalysts [6,7]. However, supported noble metal catalysts are obviously more expensive and also tend to be deactivated more quickly due to the Cl adsorption and the formation of oxychloride, leading to the loss of active species [6,8]. Therefore, transition metal oxide catalysts have been investigated and used extensively, and they are found to be more suitable for the chemical resistance to Cl-poisoning [7]. For example, V_2O_5 [9], Cr_2O_3 [8], MnO_x [10], NiO [11], CuO [12] and mixed oxides (such as perovskites) [13], all exhibit good catalytic oxidation activities. However, when used as single component, the loss of active sites (attracted by HCl and/or Cl_2) or the formation of volatile species (metal chloride or metal chloride oxide) at lower temperature may cause partial deactivation of these transition metal oxides, which may restrict the application of transition metal oxides when used alone to a certain extent [14,15]. Although ceria is often used as a support for removing the waste gas produced from the mobile car, it has also been studied for CVOCs oxidation recently [16]. Actually, CeO_2 can even be more active than supported noble metal catalysts in deep oxidation of toluene [17]. However, less consideration has been given to investigate systematically the nature of each transition metal and the suitability of various transition metal doped CeO_2 catalysts for CVOCs destruction, though several transition metal doped mixed oxides have previously been considered, such as CeO_2 MnO_x [18], CuO/CeO_2 [19], CeO_2–ZrO_2 [20] and $Ce_xPr_{1-x}O_2$ [21]. Besides, for metal oxides catalysts, the stabilization of active components and the improvement

* Corresponding author. Tel.: +86 571 88273290; fax: +86 571 88273283.
E-mail address: zhourenxian@zju.edu.cn (R. Zhou).

http://dx.doi.org/10.1016/j.apcatb.2014.06.048
0926-3373/

of chemical resistance to Cl species, need to be further developed.

The scope of this paper is to investigate systematically the catalytic performances of a series of transition metal-doped cerium catalysts for oxidative destruction of four model molecules with different structures, i.e., trichloroethylene (TCE), chlorobenzene (CB), 1,2-dichloroethane (DCE) and dichloromethane (DCM), in an attempt to understand the roles of various transition metal oxides and to obtain a more clear picture of the reaction mechanism. It focuses on evaluating the influence of the nature of each metal as well as the interaction between CeO_2 and transition metal oxides, on the activity, selectivity and stability for vapour-phase oxidation of CVOCs under dry or wet condition, and finally finding out the relationship between catalytic performance and structure information of these catalysts. The "mixture effect", i.e., the effect of the presence of water, benzene or ethyl acetate on CVOCs destruction, is also further studied.

2. Experimental

2.1. Catalysts preparation

All the mixed oxides catalysts were prepared by coprecipitation method. $Ce(NO_3)_3{\cdot}6H_2O$ and $M(NO_3)_x{\cdot}yH_2O$ were dissolved in deionized water (the atom molar ratio of Ce/M is 4:1, M = Cr, Mn, Fe, Co, Ni and Cu, respectively). For ceria-based vanadium catalyst, $VO(C_2O_4)_2$ solution was used. Then 1.0 mol L^{-1} NaOH solution was added into the above solution dropwise with rigorous stirring until the final pH value reached to 10.0. The precipitate was aged at room temperature (25 °C) for 12 h followed by filtration and washed with deionized water. The obtained precipitate was finally dried in alcohol under supercritical condition (265 °C, 7.5 MPa) for 2 h and calcined in air at 500 °C for 2 h. The catalysts were pressed into pellets, subsequently sieved to 40–60 meshes (0.3–0.45 mm) and marked as 4Ce1M (M = V, Cr, Mn, Fe, Co, Ni and Cu, respectively). For comparison, pure CeO_2 catalyst was also prepared by the same method.

2.2. Catalysts characterization

X-ray diffraction (XRD) measurement was carried out using a R-ASIX RAPID diffractometer (Rigaku Corporation, Japan) with Cu K_α radiation at 40 kV and 250 mA, in a scanning range of 10–80° (2θ). The diffraction line positions were determined with a step size of 0.02° and a counting time of 2.5 s per step.

The textural properties of these catalysts were measured by N_2 adsorption/desorption at liquid nitrogen temperature (77 K) using a Coulter OMNISORP–100 apparatus. Specific surface area was calculated using the BET and BJH methods. Before measurement, all the samples were degassed under high vacuum at 200 °C for 4 h.

The X-ray photoelectron spectroscopy (XPS) measurements were conducted on a Thermo *K*-Alpha equipped with Al *K*α radiation (1486.6 eV), operating at 84 W and with energy pass of 40 eV. Binding energies were calibrated using C 1s hydrocarbon peak at 284.6 eV.

The temperature-programmed reduction of hydrogen (H_2–TPR) was conducted in a quartz fixed-bed micro-reactor equipped with a TCD detector, using 5 vol.% H_2/Ar mixture (40 mL min^{-1}). After the catalysts were pretreated in N_2 flow (30 mL min^{-1}) at 200 °C for 30 min, the reduction process was performed from 50 to 900 °C at a heating rate of 10 °C min^{-1}.

UV-Raman spectra were obtained on a UV-HR Raman spectrograph, using the He–Gd laser of 325 nm as the excitation wavelength. The spectra acquisition consisted of 2 accumulations of 60 s for each sample, and the spectral resolution was 4 cm^{-1}. A range of 100–1000 cm^{-1} was observed.

The scanning electron microscopy (SEM) characterization was carried out on a SU1510 apparatus to get the surface profile of the samples.

2.3. Catalytic performance tests

The catalytic performance tests were performed in a traditional fixed-bed micro-reactor (quartz tube, 6 mm i.d.), in which 500 mg catalyst was used. The feed to the reactor was performed by delivering liquid CVOC into dry air using a syringe pump, and then metered by a mass flow controller. The reaction feed consisted of ~1000 ppmv each CVOC, and the operating condition was: GHSV = 15,000 h^{-1} (or 9000 mL g^{-1} h^{-1}) with a total flow of 75 mL min^{-1}. To further investigate the mixture effect, additional ~1000 ppmv benzene or ethyl acetate was injected in to the system by the same method. The water stream fed into the reaction system was carried out by bubbling air into the deionized water maintained at 20 °C. The pipeline was heated to 120 °C to minimize the possible adsorption of the CVOCs on the inner surface. After stabled at 90 °C for 1 h to reach the adsorption–desorption equilibrium, the catalysts were heated from 90 to 550 °C in steps of 20 °C to measure the catalytic activity. The gases in the outlet were analyzed on-line at given temperatures by adopting two gas chromatographs (GC), one equipped with TCD for quantitative analysis of CO_2 and CO, and the other with FID for analysis organic compounds quantitatively. When no organic compounds were detected in the outlet, the concentration of both HCl and Cl_2 was measured by bubbling the waste gases through a 0.0125 mol L^{-1} NaOH solution for 0.5 h each time. The Cl_2 concentration in the bubbled solution was measured by chemical titration with ferrous ammonium sulphate (FAS) using *N*,*N*-diethyl-*p*-phenylenediamine (DPD) as the indicator [22], and the Cl^{-1} concentration was determined by using an ion selective electrode. All the measurements were repeated three times.

Durability tests for DCE destruction were performed at given temperatures under the same condition as mentioned above, and all the catalysts used were fresh.

2.4. Temperature-programmed surface reaction (TPSR) measurement

TPSR measurement was performed under the same condition as the catalytic performance tests, in order to detect the evolutions of the reactant, the intermediates, the byproducts and the final products. TCE adsorption on the catalysts was firstly performed at 50 °C. After reaching the adsorption–desorption equilibrium, the catalyst was heated from 50 to 550 °C at the rate of 5 °C min^{-1}. The concentration of the reactant (TCE) and the products (CO_2, HCl and Cl_2) was measured on-line by using a mass spectrometer apparatus (HIDEN QJC–20).

3. Results and discussion

3.1. Catalytic performance results for catalytic degradation of various CVOCs

3.1.1. TCE degradation

The evaluation results for catalytic oxidation of TCE over CeO_2 and CeO_2-based transition metal mixed oxide catalysts under dry air condition are shown in Fig. 1. As shown in Fig. 1(A), TCE cannot be completely destroyed over pure CeO_2 even the temperature reaches to 550 °C (only 85% conversion is obtained), while the homogeneous reaction occurs only above 450 °C and TCE conversion is just 78% when the temperature reaches to

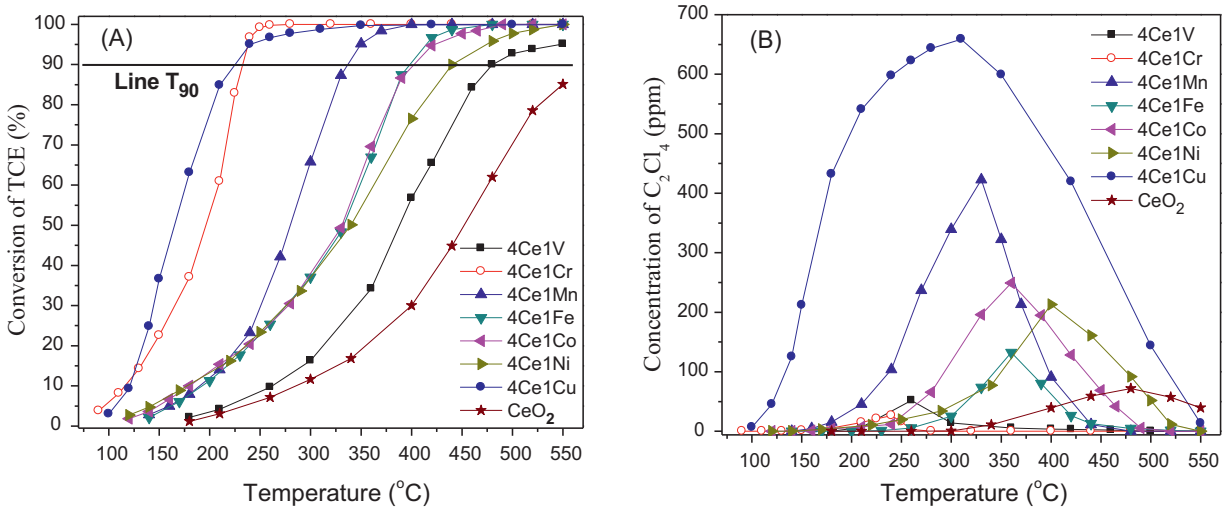

Fig. 1. Catalytic performances for TCE destruction over the catalysts in dry air: (A) TCE conversion; (B) concentration of the byproduct C_2Cl_4.

650 °C [23]. However, after doping transition metal, the catalytic activities are enhanced obviously at different levels, especially over 4Ce1Cu and 4Ce1Cr, due to the different nature of each transition metal. By comparing with the value of T_{90} (temperature at which 90% conversion is attained), the sequence of the catalytic activity for TCE destruction is as follows: 4Ce1Cu (224 °C) > 4Ce1Cr (232 °C) > 4Ce1Mn (336 °C) > 4Ce1Fe (398 °C) > 4Ce1Co (404 °C) > 4Ce1Ni (441 °C) > 4Ce1V (480 °C) > CeO_2 (>550 °C).

As shown in Fig. 1(B), C_2Cl_4 is the only byproduct detected in the waste stream during TCE decomposition. Over pure CeO_2, small concentration of C_2Cl_4 with T_{max} (temperature at which the maximum concentration reaches) at higher temperature (480 °C) is detected. After doping transition metal, the catalysts represent very different catalytic behaviors for TCE oxidation. Large concentration of byproduct C_2Cl_4 is observed over 4Ce1Cu with T_{max} (310 °C) moving to lower temperature. The formation of C_2Cl_4 is resulted from TCE chlorination followed by dehydrochlorination in presence of CuO species [24]. The chlorination reaction between TCE and Cl_2 to form the byproduct C_2Cl_4 is enhanced significantly over 4Ce1Cu, due to the promoted formation of Cl_2 via the Deacon reaction ($HCl + O_2 \rightarrow H_2O + Cl_2$) and the formation of $CuCl_x$ on the catalyst surface. Therefore, much more Cl_2 are detected, as shown in Table 1. But C_2Cl_4 is more difficult to be oxidized than TCE, thus, much higher concentration of C_2Cl_4 are detected over 4Ce1Cu. There also exists some C_2Cl_4 over 4Ce1Mn, 4Ce1Fe, 4Ce1Co and 4Ce1Ni. However, only trace of C_2Cl_4 with T_{max} (240 °C) observed at lower temperature is produced over 4Ce1Cr, indicating that the strong interaction between CrO_x and CeO_2 can result in more positive effect on the further deep oxidation of C_2Cl_4, probably due to the existence of abundant active oxygen species with better mobility as well as the presence of Cr_2O_3 species especially Cr^{6+} with stronger oxidizing ability [25]. The sequence of the peak concentrations for the byproduct C_2Cl_4 is as follows: 4Ce1Cu (659 ppm, 310 °C) > 4Ce1Mn (423 ppm, 330 °C) > 4Ce1Co (249 ppm, 360 °C) > 4Ce1Ni (213 ppm, 400 °C) > 4Ce1Fe (132 ppm, 360 °C) > CeO_2 (72 ppm, 480 °C) > 4Ce1V (52 ppm, 260 °C) > 4Ce1Cr (26 ppm, 240 °C). Moreover, all the 4Ce1M catalysts represent more than 99.5% selectivity to CO_x (more than 99% CO_2 and trace of CO) when all the organic compounds are completely destroyed.

For catalytic oxidation of TCE, the ideal reaction is (1), and the final products are CO_2, HCl and Cl_2. Cl_2 can also be formed through the Deacon reaction (2) in the presence of excess oxygen, and HCl is the thermodynamically favored product at higher temperature [2]. This result suggests that for deep oxidation of CVOCs with low H/Cl ratios, the potential for toxic products (such as Cl_2) must also be recognized since the lack of H atom to form HCl.

$$Cl_2C{=}CHCl + 2O_2 \rightarrow 2CO_2 + HCl + Cl_2 \quad (1)$$

$$2HCl(g) + 0.5O_2(g) \rightarrow H_2O(g) + Cl_2(g), \quad \Delta G_{298} = -38.0\,\text{kJ mol}^{-1}; \quad \Delta H_{298} = -57.2\,\text{kJ mol}^{-1} \quad (2)$$

Based on previous literatures [26,27], the mechanism for deep oxidation of TCE over catalysts is known below. TCE firstly interacts with surface OH groups of the catalyst through dehydrochlorination to form acyl chloride, which is further oxidized into H_2O and CO_x in the presence of active oxygen species. At the same time, the byproduct C_2Cl_4 can also be formed via TCE chlorination followed by dehydrochlorination in the presence of MCl_x or Cl_2 on the catalyst or in the reaction system. Therefore, deep catalytic oxidation of TCE contains two parallel reaction, and the second reaction route (leading to the formation of the byproduct C_2Cl_4) contains two consecutive reaction (TCE to C_2Cl_4 and finally to CO_x) [24]. Combined with the results of the experiment, it can be speculated that more acid sites (Lewis acids and OH groups) on the surface of the catalysts can favor the dehydrochlorination of TCE, meanwhile the better redox properties of the catalysts can further promote the deep oxidation of acyl chloride species into CO_x and H_2O. In the case of C_2Cl_4 production, the values of C_{max} for 4Ce1V and 4Ce1Cr are much lower than those for CeO_2 and other 4Ce1M catalysts, which may be related to that it is not easy to occur for the Deacon reaction ($HCl + O_2 \rightarrow H_2O + Cl_2$) over 4Ce1V and 4Ce1Cr (as shown in Table 1, less Cl_2 are detected). Moreover, the existence of abundant active oxygen species with better mobility and particular the presence of Cr^{6+} species with much higher oxidizing ability [25], can promote the rapid deep oxidation of both TCE and C_2Cl_4 into CO_x, HCl and Cl_2.

The data of S_{Cl_2} (the selectivity to Cl_2 when all the organic compounds are destroyed) for all these catalysts is shown in Table 1. The sequence of the peak concentration for the byproduct C_2Cl_4 is in accordance with the order of S_{Cl_2}. Since C_2Cl_4 is presumably generated by TCE chlorination followed by dehydrochlorination, its formation can be favored if reactive Cl_2 exists in large quantities [26]. As to the 4Ce1Mn, 4Ce1Fe, 4Ce1Co, 4Ce1Ni and 4Ce1Cu catalysts, much larger amount of C_2Cl_4 is detected, and it may be connected with the formation of poly metal chlorides (M_xCl_y or $M_xO_yCl_z$) on the surface of the catalysts, leading to the accumulation of Cl species and the formation of larger amount of C_2Cl_4.

Table 1
SCl2 and characterization data of the catalysts.

Catalyst	S_{Cl_2} (%)	Lattice parameter (Å)	Crystallite size (nm)	S_{BET} ($m^2\ g^{-1}$)	Pore volume ($cm^3\ g^{-1}$)	I_{587}/I_{450}
CeO_2	44.5	5.413	12.8	12.9	0.05	0.55
4Ce1V	38.2	5.412	9.2	67.1	0.31	0.69
4Ce1Cr	31.5	5.392	6.7	105.9	0.38	0.73
4Ce1Mn	59.4	5.381	5.4	111.2	0.47	0.67
4Ce1Fe	44.5	5.392	5.3	86.3	0.30	0.64
4Ce1Co	54.4	5.409	6.7	94.0	0.34	0.80
4Ce1Ni	48.5	5.410	6.4	108.7	0.56	0.62
4Ce1Cu	61.3	5.396	6.7	98.2	0.19	0.64

Moreover, the carbon balance is (96 ± 2)%, while the chlorine balance is just (80 ± 5)%, due to the deposition of Cl species on the surface of the catalysts. Based on the result of the O_2-TG-MS measurement (a MS apparatus is used to detect the signals of the gases in the outlet for the O_2-TG measurement), the chemical adsorbed Cl species can be removed above 335 °C. The Cl content is 0.40 wt% on the surface of 4Ce1Cr, confirming the accumulation of Cl on the catalyst surface, which leads to the loss of Cl in the outlet.

In order to further investigate the oxidation behavior of each transition metal, 1Ce4M catalysts (the atom molar ratio of Ce/M was 1:4) were also prepared by the same method as 4Ce1M, and their catalytic activities for TCE destruction were evaluated. The results are shown in the Supplementary material (Fig. S1). It shows that each metal has its own special property, and the oxidation activities of the 1Ce4M catalysts are in accordance with the order for TCE destruction over 4Ce1M catalysts, among which the catalyst with Ce–Cr double components exhibits the best catalytic performance.

Moreover, various kinds of CVOCs with different molecular structures may have different decomposition mechanisms over the catalysts [28–30]. A catalytic oxidation process, if properly designed, must completely destroy all kinds of CVOCs at the same time, including the harmful intermediates or byproducts produced from the incomplete combustion of the starting materials. Therefore, pure CeO_2 and 4Ce1Cr catalysts are further evaluated in term of deeper oxidation of CB, DCE and DCM below. For comparison, the oxidation behaviors of 1Ce4M catalysts for CB, DCE and DCM destruction are also evaluated, and the results are shown in the Supplementary material (Figs. S2–S4). It displays that the catalytic activity of the different catalysts for CVOCs destruction depends on the nature of the transition metal used, and Cr element exhibits the best catalytic performance.

3.1.2. CB, DCE and DCM degradation

Previous "blank test" (homogeneous reaction) shows that low concentration of CVOC reactant (CB, DCE or DCM) cannot be completely destroyed even the temperature reaches to 500 °C. As shown in Fig. 2(A), compared with pure CeO_2, the catalytic activities for CB, DCE and DCM destruction (each compound destroyed as single component every time) are all enhanced obviously over 4Ce1Cr, and the values of T_{90} decrease 195 °C, 70 °C and 95 °C, respectively. As shown in Fig. 2(B), notable amounts of dichlorobenzene-*m* and dichlorobenzene-*o* are detected over pure CeO_2 in the process of CB oxidation, C_2H_3Cl for the destruction of DCE, and CH_3Cl for DCM degradation. Interestingly, few byproducts are detected over 4Ce1Cr catalyst. The results indicate that the catalytic performances of 4Ce1Cr for deep oxidation of various CVOCs are preferable than those of CeO_2, which can be ascribed to the formation of Ce–Cr mixed oxides and the high dispersion of Cr species on the surface (see the results of the XRD analysis), as well as the formation of Cr^{6+} species with strong oxidizing ability (see the results of the H_2-TPR measurement).

Durability tests for DCE oxidation are also performed at given temperatures (shown in Fig. 3). The results display that both CeO_2 and Ce–Cr catalysts show stable conversion at higher temperatures during the 100 h test continuously, indicating that these catalysts are suitable for deep oxidation of CVOCs. Moreover, the durability test of 4Ce1Cr catalyst is further investigated. At 200 °C, DCE conversion drops rapidly in the first hour, and then, decreases slowly in the rest time. The similar situation is observed at 250 °C. While above 265 °C, no significant deactivation is observed. It is worth noticing that for the deactivated catalyst, its activity can be completely recovered after treating in dry air at 400 °C for 2 h, but can only be recovered partially when the treating temperature is 300 °C. The deactivation found at lower temperatures may be related to the chemical adsorption of Cl species produced in the process of DCE

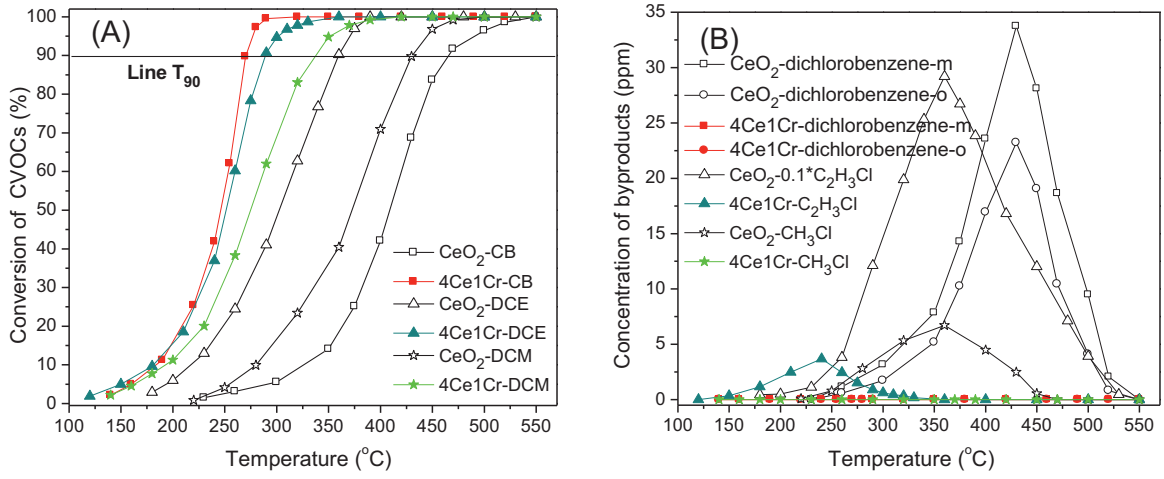

Fig. 2. Catalytic performances for CVOCs destruction over the catalysts in dry air: (A) conversion of CVOCs; (B) concentration of byproducts.

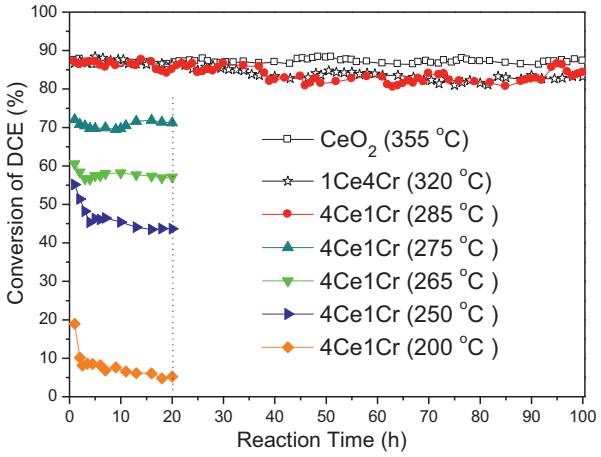

Fig. 3. Durability test for DCE destruction in dry air over the catalysts.

destruction on the surface of the catalyst [18], as well as the slight CO_2 adsorption (see Fig. 11), thus blocking part of active sites.

3.1.3. *Influence of water on the catalytic performances of 4Ce1Cr catalyst for various CVOCs destruction*

In practice, water is also present in the effluent streams, and its concentration can easily exceed the concentration of CVOCs. The presence of water in the gaseous stream may have significant effects on the destructive properties and products distribution. Thus, CVOCs conversions over 4Ce1Cr catalyst are also evaluated in the presence of water and the results are shown in Fig. 4. Results show that the T_{90} for catalytic oxidation of these CVOCs with different chemical nature are all below 310 °C in the presence of water, indicting the high catalytic performances of 4Ce1Cr catalyst. For deep oxidation of TCE, CB, DCE and DCM, T_{90} is classified as 232, 270, 288 and 337 °C without water presence and as 247, 295, 290 and 310 °C with water presence, respectively. Water inhibits TCE and CB combustion, promotes DCM oxidation, whereas has little effect on DCE destruction. This phenomenon shows that water affects CVOCs combustion over 4Ce1Cr catalyst in a complicated way, and significant "mixture effect" should be noticed when a given chlorinated feed was oxidized in the presence of water. Water could inhibit the conversion of CVOCs over catalysts at low temperature due to its competitive adsorption on active sites, but promote at high temperature via the removal of surface Cl and C species [31]. Moreover, in present of water, only slight byproducts were detected in the

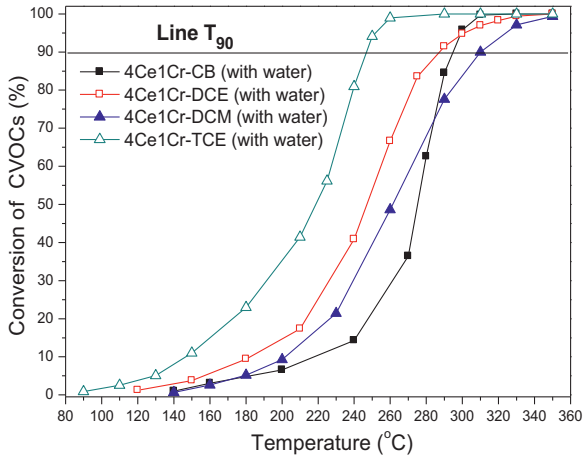

Fig. 4. Catalytic performances for CVOCs destruction over 4Ce1Cr catalyst under wet condition (2.3% H_2O).

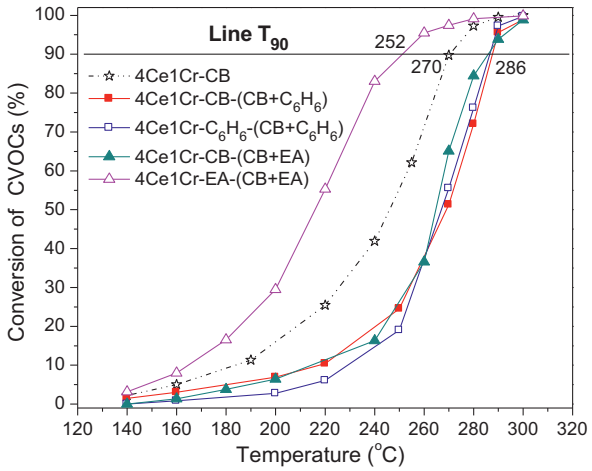

Fig. 5. Catalytic performances for CB destruction (1000 ppm) over 4Ce1Cr catalyst in the presence of benzene (1000 ppm) or ethyl acetate (1000 ppm).

process of DCE and TCE oxidation (the maximum concentration were ~7 ppm for C_2H_3Cl and ~12 ppm for C_2Cl_4, respectively), while no byproducts were detected for CB and DCM destruction. Removing Cl species away from the surface (mainly in the form of HCl) by water is responsible for reducing the formation of these byproducts.

3.1.4. *Influence of non-chlorinated VOCs on the catalytic performances of 4Ce1Cr catalyst for CB destruction*

Generally, VOCs such as hydrocarbons and oxygenated VOCs are also present in the effluent streams containing CVOCs. The presence of these VOCs in most cases can affect the light-off characteristics of CVOCs. Thus, the effects of benzene and ethyl acetate (EA) on CB destruction were also investigated and the results were shown in Fig. 5. In the present of benzene or EA, the curves for CB destruction were shifted to moderately higher temperatures (16 °C higher), while no byproducts were detected. This result indicates that the presence of such VOCs can slightly decrease CB conversion at low temperature. The increased combustion temperatures for CB destruction suggests that benzene or EA competes for active sites [32], leading to the attenuation of catalytic activity for CB destruction. The additional heat and hydrogen supplement in such VOCs combustion may contribute to accelerating the oxidation rate to some extent, but competitive adsorption for the active sites appears to be the major factor, since CB can be completely destroyed at relatively low temperature.

It is worth noting that in the presence of benzene or EA, the T_{90} for CB oxidation are all below 300 °C in spite of a little decrease of conversion compared with the absence of these compounds, indicting the high catalytic performances of 4Ce1Cr catalyst, which are even higher than noble metal [28]. Moreover, benzene and EA can also be completely oxidized below 300 °C over 4Ce1Cr catalyst in the presence of CB. Particularly for EA oxidation, the activity of 4Ce1Cr is higher than noble metal [33], while EA is one of the most difficult organic compounds to oxidize over Pt-based catalysts.

3.2. *Catalyst characterization*

3.2.1. *Texture/structure characterization*

XRD patterns of CeO_2 and 4Ce1M catalysts are displayed in Fig. 6, and Table 1 lists the lattice parameter and corresponding crystallite size. From Fig. 6, we can see that the feature diffraction peaks of cubic CeO_2 (fluorite structure of CeO_2 at 28.6°, 33.3°, 47.6° and 56.4°) [17,20] appear on all the catalysts studied, revealing the formation of large crystallites of CeO_2, and the doping of transition

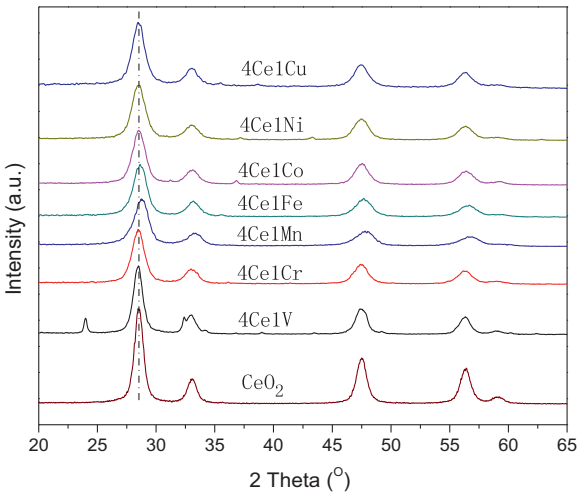

Fig. 6. XRD patterns of the catalysts.

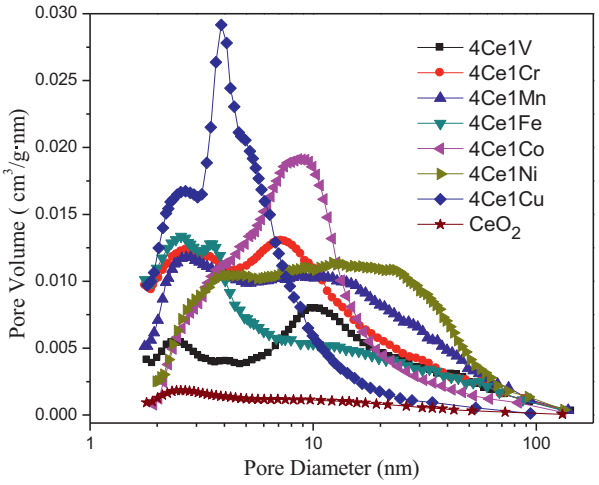

Fig. 7. Pore-size distribution of the catalysts.

metal oxide with low amount has not changed the framework of CeO_2. Moreover, the diffraction peaks of the 4Ce1M catalysts shift to different values of Bragg angles in the range of 28.5–28.8, indicating that some of transition metal ions may go into the fluorite lattice, which contributes to improving the stability of active components. Since the ionic radius of 3d-transition metal (0.05 nm–0.07 nm) are smaller than that of Ce^{4+} ion (0.094 nm), the doping of transition metal into the fluorite lattice would lead to the shrinkage of the crystal cell of CeO_2 (shown in Table 1). The lattice parameters of 4Ce1Mn, 4Ce1Fe and 4Ce1Cr catalysts are much smaller than those of pure CeO_2, indicating that more Mn, Fe and Cr are doped into the fluorite lattice. In addition, the crystallite dimensions of the CeO_2 particles are also decreased to be in the nano-crystalline range of 5.3–9.2 nm after transition metal is added. For 4Ce1M catalysts, except for 4Ce1V and 4Ce1Mn, the feature diffraction peaks of Cr_2O_3 [34,35], Fe_2O_3 [36], CoO [37], NiO [38] and CuO [39] are rather weak, indicating a relatively homogeneous dispersion of these transition metal oxides on CeO_2 and some of the transition metal components may combine with Ce to form CeO_2–MO_x mixed oxides. While for 4Ce1V, the stronger characteristic peaks of V_2O_5 (33.6°, 36.3° and 54.9°) [40] are observed, which means the vanadium oxide easily aggregates on the surface of ceria. No distinct diffraction peaks ascribed to MnO_x can be observed, probably due to the high dispersion of Mn species into the matrix of CeO_2 [10]. The above results indicate that transition metals can go into the lattice of CeO_2, which contributes to enhancing the interaction between CeO_2 and MO_x and further improves the catalytic performances for deep oxidation of CVOCs.

The pore size distribution curves of pure CeO_2 and 4Ce1M catalysts are shown in Fig. 7, and the corresponding values of the specific surface area and pore volume are listed in Table 1. As shown in Fig. 7, all the catalysts show mesoporous structures. The pore-size distribution of these catalysts is not uniform, and the range of it is quite wide (2–80 nm). As listed in Table 1, compared with pure CeO_2, the BET specific surface areas of the transition metal-doped catalysts are all increased significantly. Moreover, the mesopore volume of 4Ce1M mixed oxides is significantly larger than that of pure CeO_2, which can promote the adsorption and activation of CVOCs molecules on the internal surface of these catalysts.

3.2.2. SEM characterization

Scanning electron micrographs of pure CeO_2 and 4Ce1Cr catalyst are presented in Fig. 8. From Fig. 8, we can see that the catalysts show different morphological structures. 4Ce1Cr catalyst exhibits rice-particle-like morphological structures with inhomogeneous particles, and most of them seem to have smaller particle size. While the appearance of pure CeO_2 represents snow-like crystals with larger particle size, which is quite different from 4Ce1Cr.

3.2.3. UV-Raman characterization

Being sensitive to crystal symmetry, Raman spectroscopy technique is considered as a useful tool to provide additional structural

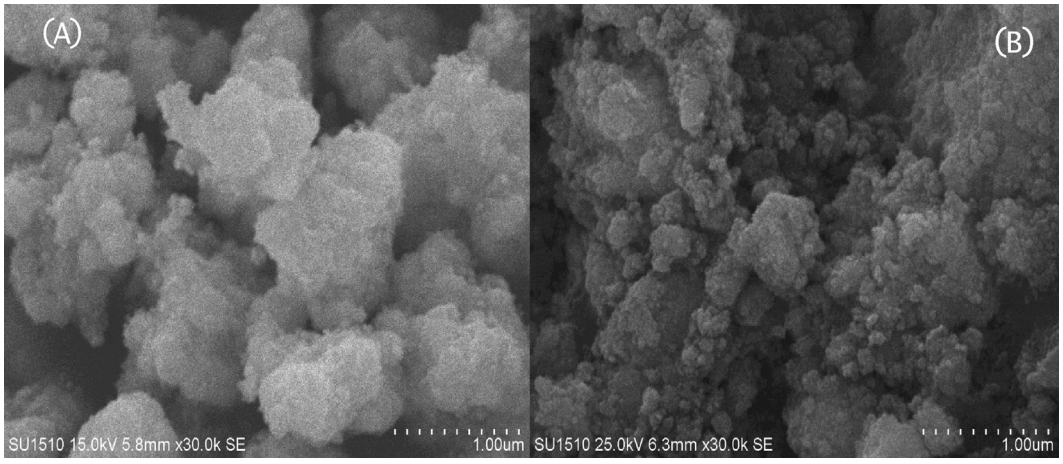

Fig. 8. SEM micrographs of CeO_2 (A) and 4Ce1Cr (B).

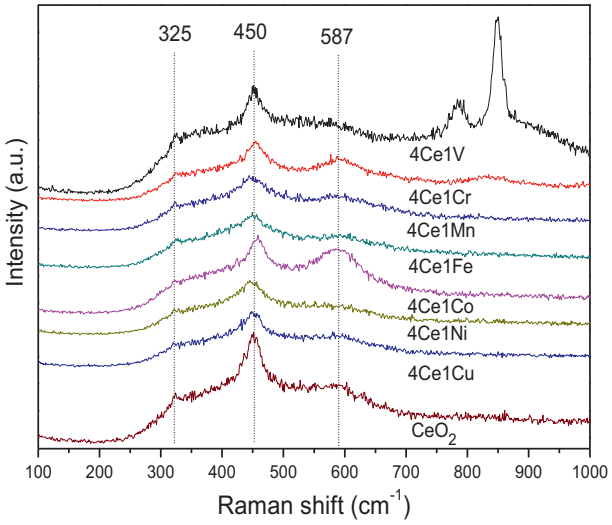

Fig. 9. UV-Raman spectra of the catalysts.

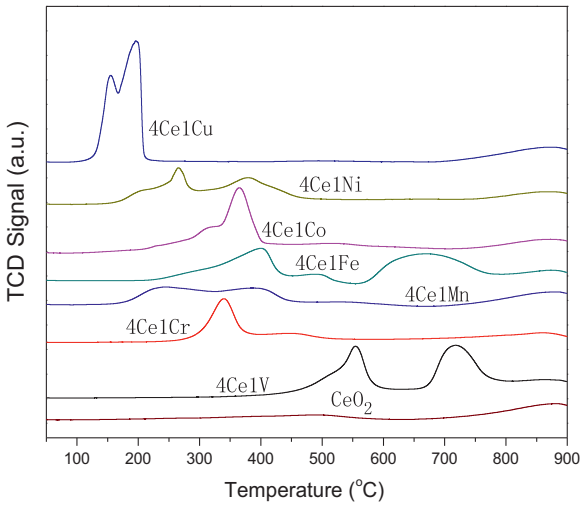

Fig. 10. H_2–TPR profiles of the catalysts.

information. Fig. 9 shows the Raman spectra of pure CeO_2 and 4Ce1M. All the catalysts (except for 4Ce1V) maintain a cubic phase due to the existence of a strong peak at 450 cm^{-1}, which is assigned to the F_{2g} Raman vibration mode of the cubic fluorite-structure phase [41]. No Raman lines attributed to transition metal oxides (except for V_2O_5) could be observed owing to a relatively homogeneous dispersion of these transition metal oxides on CeO_2 and their incorporation into the lattice of CeO_2. Besides, the central locations of strong bands deviate from the 460 cm^{-1} of pure CeO_2, also indicating that some ions are doped into the lattice of CeO_2. The reason is that the doped ions into the lattice of CeO_2 can induce the lattice to be distorted, which further influence the polarizability of the symmetrical stretching mode of [Ce–O_8] vibrational unit and lead to the shift from that in pure CeO_2 [42]. While for 4Ce1V, crystalline V_2O_5 at 794 and 856 cm^{-1} is observed. These results are consistent with the results of XRD analysis. In addition to F_{2g}-like contribution, two new bands at around 325 and 587 cm^{-1} are observed for all the samples. The band at 587 cm^{-1} is attributed to the non-degenerate LO mode of CeO_2 due to the relaxation of symmetry rules, which is often linked to the oxygen vacancies in CeO_2 lattice. The appearance of the weak band at 325 cm^{-1} can be assigned to the displacement of oxygen atoms from their ideal fluorite lattice positions [43], indicating the appearance of the defect structure as well. Under the same determination condition, the relative concentration of oxygen vacancies in the CeO_2-based mixed oxides can be represented by the intensity ratio of the bands at 587 and 450 cm^{-1} (I_{587}/I_{450}). As shown in Table 1, it is obvious that the values of I_{587}/I_{450} for CeO_2-based mixed oxides are all bigger than that of pure CeO_2, suggesting that there exist more oxygen vacancies due to the doping of transition metal oxides. This may be due to that some transition metal ions are incorporated into the ceria lattice, leading to the formation of more Ce^{3+} ions and oxygen vacancies around the Ce^{4+} ions in the lattice, which is in favor of the redox reaction of the catalysts.

3.2.4. Redox property

The results of H_2–TPR measurement for pure CeO_2 and 4Ce1M catalysts are shown in Fig. 10. The reduction of pure CeO_2 occurs at 490 °C and 880 °C, associated with the reduction of surface Ce^{4+} ions and bulk oxygen [16,20], respectively. For 4Ce1M catalysts, the reduction peaks below 800 °C mainly result from the reduction of MO_x species belonging to different phases/structures. Generally, the peak at lower temperature can be assigned to the reduction of highly dispersed metal oxides species strongly interacting with the ceria surface, such as CuO [39,44], MnO_2/Mn_3O_4 [10,18,44], NiO [37,44], CrO_3 [35,44–46], Co_2O_3 [37], Fe_3O_4 [36,44] and V_2O_5 [40,46], while the peak at higher temperature may be related to the combined reduction of MO_x species with larger particles or their intermediates as well as the removal of surface oxygen of ceria. The intensity and temperature of the reduction peaks are observed to be closely related to the diverse nature of MO_x. Among them, 4Ce1Cu catalyst is the most reducible, while 4Ce1V catalyst is the least reducible. The reducibility of the corresponding samples is in the order of 4Ce1Cu > 4Ce1Mn > 4Ce1Ni > 4Ce1Cr > 4Ce1Co > 4Ce1Fe > 4Ce1V, CeO_2. However, according to the reported literature [47], the reduction temperatures of MO_x species in 4Ce1M catalysts are much lower than those of pure MO_x, indicating that the strong interaction between CeO_2 and MO_x can improve the mobility of active oxygen species on the surface, which is beneficial for the destruction of the reactants and byproducts produced in the process of CVOCs oxidation. According to the results of the catalytic performances for TCE destruction (shown in Fig. 1), the catalytic activities of these catalysts are basically in line with their redox properties, though there exists the exception of 4Ce1Cr. The strong interaction between CeO_2 and CrO_x species can increase the amount of Cr^{6+} species with strong oxidizing ability (account for 35.4% of the total Cr content, calculated from the H_2 consumption, using known amounts of CuO as reference), which can significantly promote the deep oxidation of various CVOCs.

The quantification of Cr species (both Cr^{3+} and Cr^{6+}) on the 4Ce1Cr surface has also been analyzed by XPS measurement. The Cr 2p XPS spectra reveals two peaks at ~577.8 eV for Cr(III) and ~586.7 eV for Cr(VI), respectively. The results show that there exists 1.74 At.% for Cr^{3+} and 1.01 At.% for Cr^{6+}, which is consistent with the result of H_2–TPR measurement and further confirms the existence of Cr^{6+} species.

3.2.5. TPSR characterization

The adsorption–desorption properties of TCE and the evolution of the final products (HCl, Cl_2 and CO_2) over pure CeO_2 and 4Ce1Cr have been further studied by TPSR method, in order to evaluate the adsorption capacity of the catalysts and the selectivity to Cl_2 and CO_2 under dynamic state (shown in Fig. 11). It can be seen from Fig. 11(A) that under the same condition, the time needed from the initial to the adsorption–desorption equilibrium of TCE over the catalysts is different from each other, 12.5 min for pure CeO_2, while 18.5 min for 4Ce1Cr. This demonstrates that 4Ce1Cr has larger adsorption capacity, which mainly due to its larger BET

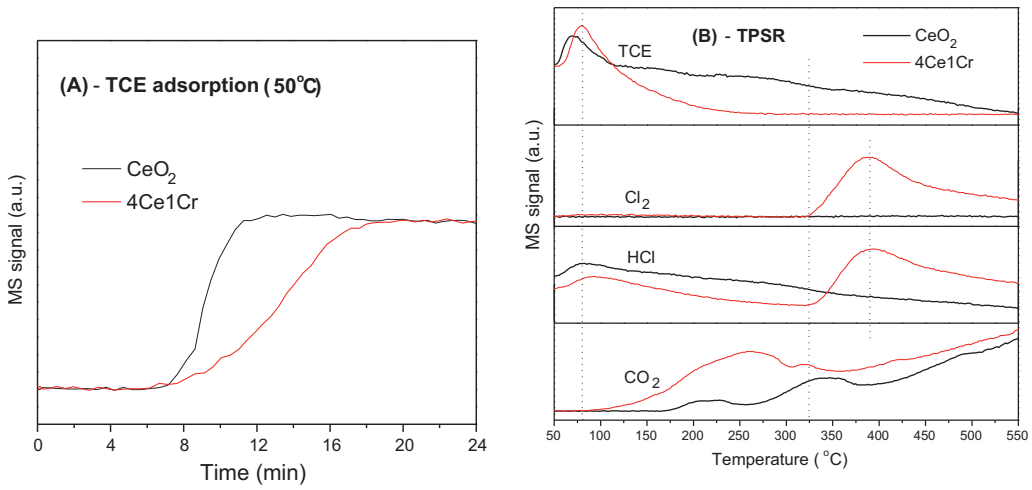

Fig. 11. TPSR profiles for TCE destruction over CeO_2 and 4Ce1Cr catalysts.

surface area and pore volume. As shown in Fig. 11(B), TCE desorption occurs at relatively lower temperature and desorption is accompanied with the destruction of TCE. TCE can be completely destroyed over 4Ce1Cr at as low as 260 °C, while it needs 550 °C for pure CeO_2. It is notable that the temperature for the desorption peak over 4Ce1Cr catalyst is higher than that over pure CeO_2, indicating that the strong interaction between CrO_x and CeO_2 enhances the adsorption of TCE. Moreover, it can be seen from the CO_2 evolution that CO_2 production over 4Ce1Cr catalyst is increased obviously compared to that over pure CeO_2 before 350 °C. Meanwhile, CO_2 can be detected as low as 100 °C over 4Ce1Cr catalyst, while it cannot be observed until the temperature is above 170 °C over pure CeO_2. This suggests that the interaction between CeO_2 and CrO_x can promote the deeper oxidation of TCE and increase the selectivity to CO_2 formation. In addition, two stronger peaks are observed over the catalysts below 380 °C, which can be assigned to a combined signal of CO_2 produced during TCE destruction and the desorption of CO_2 adsorbed at low temperatures on the surface of the catalysts [24].

As to the curves of HCl and Cl_2, the obvious peaks observed over CeO_2 and 4Ce1Cr in low temperature range (50–325 °C) can be assigned to the physical desorption of HCl, while no peaks appear for Cl_2. It is noticeable that little HCl and Cl_2 are detected over CeO_2 even the temperature reaches to 550 °C, which may be related to the strong chemical adsorption of Cl species on the surface of CeO_2 [16]. However, it is clearly seen that the desorption of HCl and Cl_2 increases obviously along with the rise of temperature above 325 °C for 4Ce1Cr due to its strong oxidizing ability, which is of great importance to reduce the Cl-posiong. Therefore, the loss of Cl species for the calculation of Cl balance, can be interpreted due to the adsorption of partial Cl species on the surface of 4Ce1Cr at low temperature.

4. Conclusions

A series of transition metal-doped cerium catalysts (4Ce1M) were synthesized by coprecipitation method and investigated in deep oxidation of chlorinated VOCs. Structure/texture characterization show that these transition metal oxides are relatively homogeneous dispersed on CeO_2 and some of transition metal ions can go into the fluorite lattice, which contributes to enhancing the stability of active components, while the vanadium oxide easily aggregates on the surface of ceria. Compared with pure CeO_2, 4Ce1M mixed oxides show mesoporous structures (pore-size distribution of 2–80 nm), and possess larger specific surface area and pore volume, which are in favor of the adsorption and activation of CVOCs molecules on the internal surface of these catalysts. Moreover, the interaction between CeO_2 and MO_x can improve the mobility of the active oxygen species on the surface and the reducibility of MO_x species, which facilitates the destruction of the reactants and byproducts at lower temperature in the process of CVOCs oxidation. Especially for 4Ce1Cr catalyst, the stronger interaction between CeO_2 and CrO_x can increase the amount of Cr^{6+} species with stronger oxidizing ability, which can avoid coke deposition and improve the chemical resistance to Cl-poisoning due to its preferable redox property. Consequently, the catalyst with Ce–Cr double components exhibits the best catalytic performances for CVOCs oxidation. Moreover, the addition of water can affect CVOCs combustion over 4Ce1Cr catalyst in a complicated way, and significant "mixture effects" are observed when a given chlorinated feed is destroyed in the presence of water. Water can inhibit TCE and CB combustion, promote DCM oxidation, whereas have little effect on DCE conversion. Water inhibits the conversion of CVOCs over catalysts at low temperature due to its competitive adsorption on the active sites, but promote at high temperature via the removal of surface Cl species. In addition, the presence of benzene or ethyl acetate can slightly decrease CB conversion due to the competition for active sites at low temperature.

Acknowledgements

We gratefully acknowledge the financial supports from Nature Science Foundation of China (no. 21177110) and Zhejiang Leading Team of Science and Technology Innovation (no. 2009R50020).

Appendix A. Supplementary data

Supplementary data associated with this article can be found, in the online version, at http://dx.doi.org/10.1016/j.apcatb.2014.06.048.

References

[1] Commission of the European Communities, COM, Thematic strategy on air pollution, in: Communication from the Commission to the Council and The European Parliament: COM (2005) 446 Final, Commission of the European Communities, Brussels, 2005.
[2] G. Erlt, H. Knözinger, F. Schüth, J. Weitkamp (Eds.), Handbook of Heterogeneous Catalysis, second ed., Wiley-VCH, Weinheim, 2008, pp. 2385–2411.
[3] A. Śrębowata, R. Baran, D. Łomot, D. Lisovytskiy, T. Onfroy, S. Dzwigaj, Appl. Catal., B: Environ. 147 (2014) 208–220.

[4] H.J. Sedjame, C. Fontaine, G.J.B. Lafaye Jr., Appl. Catal., B: Environ. 144 (2014) 233–242.
[5] A.C. Gluhoi, B.E. Nieuwenhuys, Catal. Today 119 (2007) 305–310.
[6] S.H. Taylor, C.S. Heneghan, G.J. Hutchings, I.D. Hudson, Catal. Today 59 (2000) 249–259.
[7] J.J. Spivey, Ind. Eng. Chem. Res. 26 (1987) 2165–2180.
[8] H. Rotter, M.V. Landau, M. Herskowitz, Environ. Sci. Technol. 39 (2005) 6845–6850.
[9] K. Everaert, M. Mathieu, J. Baeyens, E. Vansant, J. Chem. Technol. Biotechnol. 78 (2003) 167–172.
[10] N. Watanabe, H. Yamashita, H. Miyadera, S. Tominaga, Appl. Catal., B: Environ. 8 (1996) 405–415.
[11] M. Chen, X.M. Zheng, J. Mol. Catal. A: Chem. 221 (2004) 77–80.
[12] Y.M. Kang, B.Z. Wan, Appl. Catal., A: Gen. 114 (1994) 35–41.
[13] S. Maghsoodi, J. Towfighi, A. Khodadadi, Y. Mortazavi, Chem. Eng. J. 215–216 (2013) 827–837.
[14] R. Rachapudi, P.S. Chintawar, H.L. Greene, J. Catal. 185 (1999) 58–72.
[15] S. Krishnamoorthy, J.A. Rivas, M.D. Amiridis, J. Catal. 193 (2000) 264–272.
[16] Q.G. Dai, H. Huang, Y. Zhu, W. Deng, S.X. Bai, X.Y. Wang, G.Z. Lu, Appl. Catal., B: Environ. 117–118 (2012) 360–368.
[17] C.H. Wang, S.S. Lin, Appl. Catal., A: Gen. 268 (2004) 227–233.
[18] X.Y. Wang, Q. Kang, D. Li, Appl. Catal., B: Environ. 86 (2009) 166–175.
[19] X.D. Ma, X. Feng, X. He, H.W. Guo, L. Lv, J. Guo, H.Q. Cao, T. Zhou, Microporous Mesoporous Mater. 158 (2012) 214–218.
[20] B. de Rivas, R. López-Fonseca, M.á. Gutiérrez-Ortiz, J.I. Gutiérrez-Ortiz, Appl. Catal., B: Environ. 101 (2011) 317–325.
[21] B. de Rivas, N. Guillén-Hurtado, R. López-Fonseca, F. Coloma-Pascual, A. García-García, J.I. Gutiérrez-Ortiz, A. Bueno-López, Appl. Catal., B: Environ. 121–122 (2012) 162–170.
[22] A.E. Greenberg, L.S. Clesceri, A.D. Eaton (Eds.), Standard Methods for the Examination of Water and Wastewater, 18th ed., American Public Health Association, Washington, 1992, p. 4.43.
[23] L. Intriago, E. Díaz, S. Ordóñez, A. Vega, Microporous Mesoporous Mater. 91 (2006) 161–169.
[24] Q.Q. Huang, X.M. Xue, R.X. Zhou, J. Mol. Catal. A: Chem. 344 (2011) 74–82.
[25] P. Yang, X.M. Xue, Z.H. Meng, R.X. Zhou, Chem. Eng. J. 234 (2013) 203–210.
[26] A. Aranzabal, J.L. Ayastuy-Arizti, J.A. González-Marcos, J.R. González-Velasco, J. Catal. 214 (2003) 130–135.
[27] B. de Rivas, R. López-Fonseca, J.R. González-Velasco, J.I. Gutiérrez-Ortiz, Catal. Commun. 9 (2008) 2018–2021.
[28] S. Scirè, S. Minicò, C. Crisafulli, Appl. Catal., B: Environ. 45 (2003) 117–125.
[29] B. de Rivas, R. López-Fonseca, J.R. González-Velasco, J.I. Gutiérrez-Ortiz, J. Mol, J. Mol. Catal. A: Chem. 278 (2007) 181–188.
[30] L. Pinard, J. Mijoin, P. Ayrault, C. Canaff, P. Magnoux, Appl. Catal., B: Environ. 51 (2004) 1–8.
[31] R. López-Fonseca, J.I. Gutiérrez-Ortiz, M.A. Gutiérrez-Ortiz, J.R. González-Velasco, Catal. Today 107–108 (2005) 200–207.
[32] H. Windawi, Z.C. Zhang, Catal. Today 30 (1996) 99–105.
[33] P. Papaefthimiou, T. Ioannides, X.E. Verykios, Appl. Catal., B: Environ. 13 (1997) 175–184.
[34] S.K. Agarwal, J.J. Spivey, J.B. Butt, Appl. Catal., A: Gen. 82 (1992) 259–275.
[35] D.H. Cho, Y.G. Kim, M.J. Chung, J.S. Chung, Appl. Catal., B: Environ. 18 (1998) 251–261.
[36] X.M. Liao, W. Chu, X.Y. Dai, V. Pitchon, Appl. Catal., A: Gen. 449 (2012) 131–138.
[37] M.H. Kim, K.H. Choo, Catal. Commun. 8 (2007) 462–466.
[38] H.G. El-Shobaky, Appl. Catal., A: Gen. 278 (2004) 1–9.
[39] J. Li, Y.X. Han, Y.H. Zhu, R.X. Zhou, Appl. Catal., B: Environ. 108–109 (2011) 72–80.
[40] M. Wu, K.C. Ung, Q.G. Dai, X.Y. Wang, Catal. Commun. 18 (2012) 72–75.
[41] M. Thammachart, V. Meeyoo, T. Risksomboon, S. Osuwan, Catal. Today 68 (2001) 53–61.
[42] Y.S. She, Q. Zheng, L. Li, Y.Y. Zhan, C.Q. Chen, Y.H. Zheng, X.Y. Lin, Int. J. Hydrogen Energy 34 (2009) 8929–8936.
[43] R. Si, Y.W. Zhang, S.J. Li, B.X. Lin, C.H. Yan, J. Phys. Chem. B 108 (2004) 12481–12488.
[44] J.Y. Luo, M. Meng, J.S. Yao, X.G. Li, Y.Q. Zha, X.T. Wang, T.Y. Zhang, Appl. Catal., B: Environ. 87 (2009) 92–103.
[45] S.D. Yim, I.S. Nam, J. Catal. 221 (2004) 601–611.
[46] L.L. Xu, Y.F. Zhang, Y. Deng, Y.L. Zhong, S.B. Mo, G.Z. Cheng, C. Huang, Mater. Res. Bull. 48 (2013) 3620–3624.
[47] J.L. Ayastuy, E. Fernández-Puertas, M.P. González-Marcos, M.A. Gutiérrez-Ortiz, Int. J. Hydrogen Energy 37 (2012) 7385–7397.